OPEN ACCESS
JOURNAL OF ADVANCED DIELECTRICS
Vol. 11, No. 5 (2021) 2160015 (9 pages)

DOI: 10.1142/S2010135X21600158

Dielectric and piezoelectric properties of modified lead-free $NaNbO_3$–$KNbO_3$/PVDF composite ceramics

Y. I. Yurasov*,†,‡, M. I. Tolstunov†, A. V. Nazarenko*, A. A. Pavelko†, A. V. Yudin*,†, I. A. Verbenko† and L. A. Reznichenko†

*Federal Research Centre
The Southern Scientific Centre of the Russian Academy of Sciences (SSC RAS)
41 Chekhova Street, Rostov-on-Don 344006, Russia

†Southern Federal University
105/42 Bolshaya Sadovaya Street
Rostov-on-Don 344006, Russia

‡yucomp@ya.ru; yucomp@yandex.ru

Received 14 April 2021; Revised 3 June 2021; Accepted 21 June 2021; Published 18 August 2021

This work presents the results of study of the electrophysical properties of composite polymer ceramics (1–x)[KNN-LTSN]–xPVDF at $x = 25$ vol.% and $x = 50$ vol.% in the temperature range of $T = 20$–160 °C and frequency range of $f = 2 \times 10^1$–2×10^6 Hz. The concentration dependence of piezomodules of the studied materials has been analyzed as a function of temperature. X-ray measurements have also been carried out. A model of description of revealed dielectric parameters dispersion in the material is presented. The nonclassical modified Havriliak–Negami model written for complex electrical conductivity has been used to describe the temperature–frequency properties. It is shown that the dielectric spectra of the studied composites include three relaxation processes in the temperature ranges of 40–80 °C, 80–120 °C and 120–150 °C, which were confirmed by the dynamics of changes in the dependences of $\gamma'(f)$, $\mathrm{tg}\delta(f)$, $M'(f)$, $M''(f)$ and $M''(M')$. All three processes are almost exactly described by this model and well correlated with the studies by other researchers of the composites based on PVDF. The results of this work show that the use of such experimental model is suitable for describing the complex dielectric spectra of any nonlinear dielectrics including composite materials.

Keywords: Composites; PVDF; KNN; ferroelectrics; relaxation; Havriliak–Negami model; complex conductivity.

1. Introduction

In modern branches of science and technology, piezoceramic materials are widely used because of their properties. The demand, supported by numerous studies, is driven by the need for reliable, economical and efficient methods for the production of active ferroelectric materials with specific structural and physical characteristics. At the same time, piezocomposites with the addition of various polymers are often considered as objects of study. Among them, the leading role is played by polymer-based ferroactive composites, which, due to their high piezosensitivity and piezoelectric activity as well as relatively high resistance to mechanical low-frequency and shock loads, find their application in various sensors and transducers.[1–4]

Polyvinylidene fluoride (PVDF) attracts special attention as a polymer with sufficiently high values of piezoelectric and pyroelectric parameters for its class.[5] Piezocomposites based on it are among the most promising materials that combine properties such as aging resistance, chemical inertness, excellent dielectric properties, heat resistance, strength and flexibility, low friction coefficient, no adhesion, low water absorption, atmospheric and radiation resistance. The relevance of its use is confirmed by many studies in various fields, the results of which have been especially actively discussed in recent years.[6–10] For example, PVDF in combination with graphene has lower fluidity and higher viscosity, which make it possible to be successfully used in printing technology.[6] It was noted that its polar structure makes it possible to achieve rather high values of the dielectric constant (45 pC/N). If TiO_2 is added to PVDF, then its hydrophilic properties are significantly enhanced. This makes it possible to manufacture membranes capable of adsorbing up to 98% of copper particles and copper-containing impurities on themselves.[7] Studies on the use of PVDF as a basis for piezoelectric transducers with the use of additional additives in the form of nickel oxide or barium titanate deserve attention.[8,9] In addition, PVDF has excelled in the technology of manufacturing a piezoresistive system,[10] which is promising for use in flexible storage media and thin-film transistors, as well

‡Corresponding author.

as in the development of a composite polymer film used for shielding electrical equipment.[11]

Many works consider the issues of manufacturing polymer composites using lead-free piezomaterials for various applications, including for the creation of film nanogenerators,[12,13] which is due to the directives[14] limiting the use of harmful substances in the production of active elements. It should be noted that in the examples presented above, the piezoelectric properties of the material are either not high enough or are combined with low strength characteristics. In addition, their creation often requires specialized and expensive equipment for production.

The aim of this work is to obtain composite polymer ceramics based on environmentally friendly material — potassium–sodium niobate (KNN) modified with elements namely Li, Ta, Sb and NiO (KNN-LTSN) [multicomponent system (K,Na,Li)(Sb,Nb,Ta)O_3 with NiO][15,16] — using PVDF as a binder and studying their piezoelectric and dielectric characteristics using new approaches to the analysis of dielectric spectra.[17,18]

As we have shown earlier, KNN-LTSN have well proven themselves when used as an active element of knock sensors.[19–21]

2. Research Objects and Methods

A KNN-LTSN sample with a density $\rho = 4.27$ g/cm^3 and a piezomodule $|d_{33}| = 101$ pC/N prepared by traditional ceramic technology to use in knock sensors[16,19] was ground in a mortar with the addition of ethylene. To obtain composite ceramics, powders of KNN-LTSN and PVDF polymer were mixed, placed in a mold with a heating element and pressed into tablets with a diameter of 10 mm at a temperature of 180 °C and a pressure of 20 MPa for 10 min. The pressing temperature was chosen taking into account the melting point of PVDF ~170 °C.

The paper presents the results of studies of two samples of composite ceramics $(1-x)$[KNN-LTSN]–xPVDF with x = 25% and x = 50% volume fractions (vol.%), the densities and piezomodules of which were $\rho = 3.17$ g/cm^3, $|d_{33}| =$ 30 pC/N (x = 25 vol.%) and $\rho = 3.24$ g/cm^3, $|d_{33}| = 9$ pC/N (x = 50 vol.%). The electrodes were deposited in a vacuum chamber by cathode sputtering using a silver target. The samples were polarized in a dielectric liquid by a pulsed method up to 10 kV at room temperature.

The microstructure was studied on sample cross-section cleavage by confocal step-by-step scanning ($\Delta z = 0.1$ μm) using a Keyence VK-9700 3D scanning laser (408 nm) microscope at the Center for Collective Use of the SSC RAS "Joint Center for Scientific and Technological Equipment of the SSC RAS (Research, Development, Testing)". X-ray phase analysis was carried out on an ARL X'TRA powder diffractometer using Cu-Kα radiation at room temperature. Scanning speed was 5°/min.

The temperature dependences of the real (ε') and imaginary (ε'') parts of the complex relative permittivity ($\varepsilon^*/\varepsilon_0 = \varepsilon'/\varepsilon_0 - i\cdot\varepsilon''/\varepsilon_0$) were studied at different frequencies of the alternating electric field using a high-temperature furnace, PTC10 temperature controller (Stanford Research Systems) with a Pt RTD sensor, Agilent E4980A LCR meter, and a personal computer. Measurement, recording of data and calculation of parameters were carried out automatically using specially developed software. The measurements were carried out in the 20 Hz–2 MHz frequency range, and in the 20–160 °C temperature range in the regimes of monotonous heating and cooling at a rate of 1 K/min (Method No. GSSD ME 184–2011[22]). The dielectric and piezoelectric properties of polarized ceramic samples were studied on the same bench in the same conditions. In this case, relative dielectric constant of polarized samples ($\varepsilon_{33}^T/\varepsilon_0$), piezoelectric module ($|d_{31}|$), piezoelectric sensitivity ($|g_{31}|$) and mechanical quality factor (Q_M) were determined. The calculations were performed by the resonance method according to the IEEE Standards 176.[23] The values of the resonance and antiresonance frequencies were determined from impedance measurements of the samples using specially developed software. Nonlinear approximation of resonance curves was performed using the plug-in library of algorithms ALGLIB.[24]

Approximation of relaxation processes in dielectric spectra was carried out using the developed computer program[25] using a new modified model based on Havriliak–Negami to describe the dispersion of complex electrical conductivity,[17,18]

$$\gamma^* = \gamma_\infty + \sum_{n=1}^{\infty} \frac{\gamma_{Sn} - \gamma_{\infty n}}{(1 + (i\omega\tau_n)^{1-\alpha})^{1-\alpha}} + \varepsilon''_\infty \omega\varepsilon_0 + i\varepsilon'_\infty \omega\varepsilon_0, \quad (1)$$

where $\gamma^* = \gamma' + i\gamma''$ is the combined complex electrical conductivity; $\varepsilon''_\infty \omega\varepsilon_0$ is the singular term that shows the reach-through conductivity contribution in γ'; $\varepsilon'_\infty \omega\varepsilon_0$ is an additional term; ε'_∞ is a value of ε' at $\omega \to \infty$; ε''_∞ is a value of ε'' at $\omega \to \infty$; $\Delta\gamma_n = \gamma_{Sn} - \gamma_{\infty n}$; $\gamma_{Sn} = \gamma_{\infty n-1}$; n is the relaxation process number; and α is the parameter of the temperature–frequency distribution of dielectric losses ($0 \le \alpha \le 1$), which unlike other known models for describing dielectric spectra is not "fitting",[17]

$$\alpha = \frac{kT}{E_a} \ln Q_\infty, \quad (2)$$

where $Q_\infty = \varepsilon'_\infty/\varepsilon''_\infty$ is the quality factor at $\omega \to \infty$.

The values of the modules M', M'' were calculated using the following formulas:

$$M' = \frac{\varepsilon'}{\varepsilon'^2 + \varepsilon''^2}, \qquad M'' = \frac{\varepsilon''}{\varepsilon'^2 + \varepsilon''^2}. \quad (3)$$

3. Results and Discussion

The microstructures of a cross-section cleavage of studied objects are presented in Figs. 1 and 2.

It can be seen that in the case of pure KNN-LTSN (Fig. 1) the ceramic has a small porosity. The cleavage of ceramics

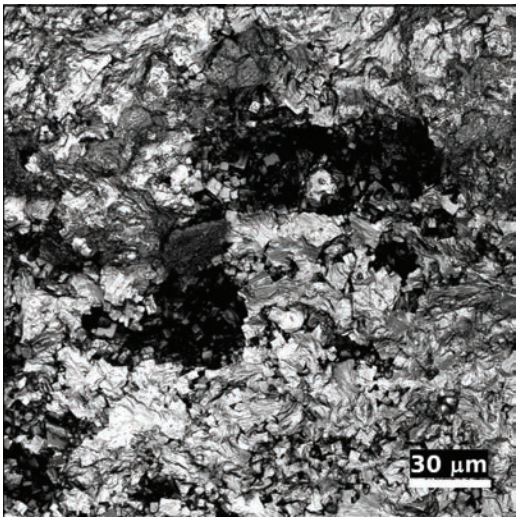

Fig. 1. Microstructure of KNN-LTSN.

passes mainly along the grains, which makes it possible to fully manifest the faceting of the crystallites. In this case, the grain boundaries are not clear. In places where pores are present, separate crystallite aggregations are clearly visible.

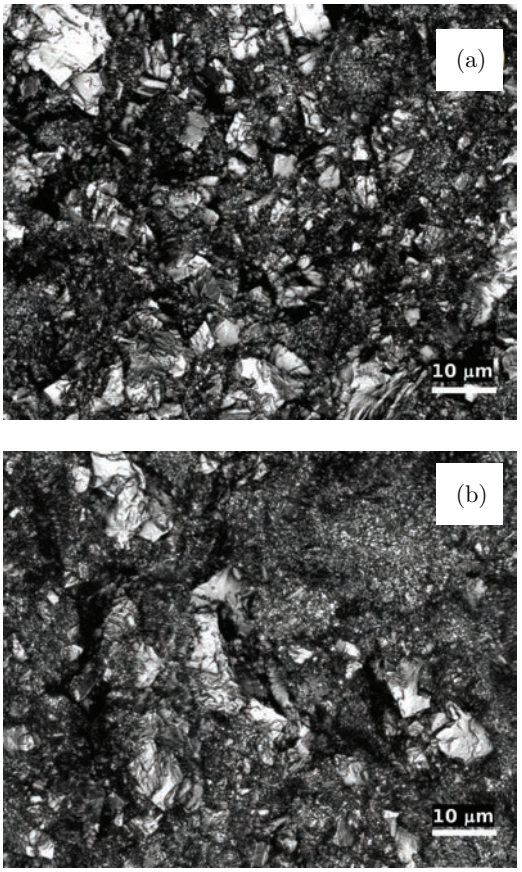

Fig. 2. Microstructures of (1–x)[KNN-LTSN]–xPVDF with (a) x = 25 vol.% and (b) x = 50 vol.%.

Note also that the grains have a predominantly regular cubic shape. All these indicate quasi-equilibrium conditions for the formation of a microstructure, probably under conditions of exchange with an amorphous melt-solution. The range of crystallite sizes is from 2.5 μm to 9 μm.

In the samples with PVDF [Figs. 2(a) and 2(b)], in both cases, the porosity is significantly reduced due to the submicron size of the polymer grains, which easily fill any empty areas when exposed to external pressure. However, due to the low density of PVDF itself, applied pressures and temperatures are not sufficient to produce a composite with a high density and, as noted above, it turned out to be ~34% lower than that of pure KNN-LTSN. The analysis of Fig. 2 shows that the fragments of crushed pure KNN-LTSN are clearly visible. In this case, the particles have an irregular shape as a result of a rather coarse grinding, therefore, the size of the fragments varies from the size of the grains themselves (~9–10 μm) to large fragments of the order of 35 μm.

It can be seen that at x = 50 vol.%, the amount of PVDF noticeably predominates in the microstructure [Fig. 2(b)]. Therefore, KNN-LTSN fragments are located at a distance significantly exceeding their linear dimensions. Obviously, in this case, the displayed properties are to a greater extent consistent with the properties of the phase with high connectivity, i.e., PVDF, while the value of the resulting piezomodule is only $|d_{33}|$ = 9 pC/N (9% of the initial KNN-LTSN). At x = 25 vol.%, the number of fragments of pure KNN-LTSN increases [Fig. 2(a)], and the distance between them significantly decreases, which provides an indirect electromechanical connection between them. In this case, the value of the obtained piezomodule is already $|d_{33}|$ = 30 pC/N (30% of the original KNN-LTSN). Higher values of the piezoelectric module can be achieved by reducing the PVDF content, as well as increasing the temperature and pressure of pressing. A decrease in the size of granules of the piezoactive phase due to, e.g., the use of the method of mechanical activation can also lead to a denser electromechanical interaction of KNN-LTSN fragments, which, along with an increase in the experimental density, will contribute to an increase in piezoelectric coefficients. The above assumptions are confirmed by the dependence of the piezomodule on the PVDF concentration $|d_{33}|(x)$ shown in Fig. 3 with the use of the literature data, which present the results of studying the properties of the $NaNbO_3$ composite with PVDF.[26]

As can be seen from the figure, the $|d_{33}|(x)$ dependence has an exponential character, which is confirmed by the approximation, which was performed by the least squares method, the corresponding results are translated in the inset of Fig. 3, and demonstrates a high degree of correlation with experimental data.

As an additional control of the composition when introducing organic matter into the KNN-LTSN samples, X-ray studies were performed. The diffractogram of a sample with x = 25 vol.% in comparison with pure KNN-LTSN is shown in Fig. 4. The positions of the Bragg peaks show that

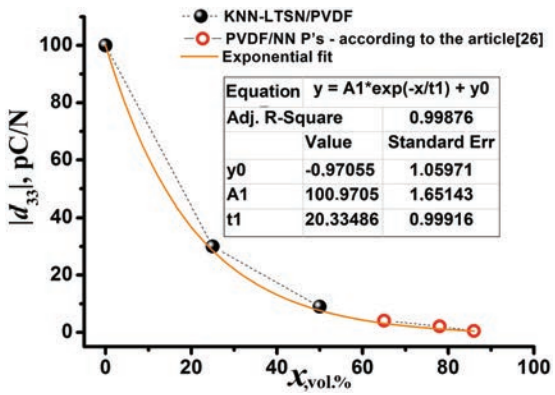

Fig. 3. Dependence of $|d_{33}|(x)$ of the studied $(1-x)$[KNN-LTSN]–xPVDF.

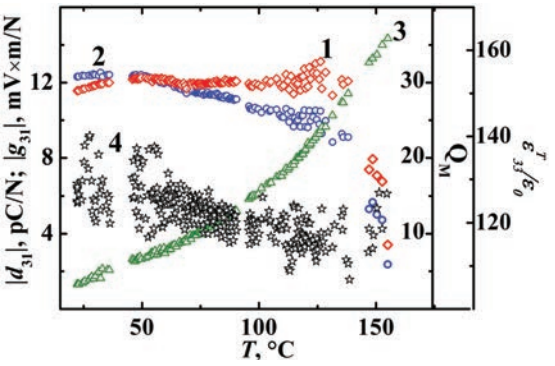

Fig. 5. The temperature dependences of the piezoelectric module, $|d_{31}|$ (1), the piezoelectric sensitivity, $|g_{31}|$ (2), the relative dielectric constant of the polarized sample, $\varepsilon_{33}^T/\varepsilon_0$ (3), measured at a frequency of 1 kHz, and the mechanical quality factor, Q_M (4), of the polarized samples.

KNN-LTSN–PVDF are two-phase materials. PVDF is represented by a reflection at $2\theta = 20°$, the rest of the reflections belong to KNN-LTSN, which has an orthorhombic structure. The reflexes do not shift, which indicates the absence of chemical interaction in the bulk of the phases of the components (Fig. 4). It should be noted that the X-ray diffraction pattern of a pure polymer contains two peaks, such as α-phase (18.4°) and β-phase (20°).[27,28] It is believed that the presence of the α-phase is the reason for the low values of the dielectric activity of PVDF due to the nonpolar chain crystalline conformation. It can be seen that in the manufacture of composite materials based on PVDF, the α-phase disappears (Fig. 4, KNN-LTSN–PVDF). Note also that the β-phase reflex is shifted to the right up to ~20.4° (inset of Fig. 4). This indicates a partial reaction of the polymer with KNN-LTSN particles, which leads to a slight decrease in its structural parameters.

Figure 5 shows the most characteristic temperature dependences of the electrophysical parameters of polarized samples. As can be seen from the figure, the $|d_{31}|(T)$ dependence passes through a small maximum at a temperature of ≈130 °C, followed by a sharp drop in piezoactivity twice in the region of 150 °C. This behavior is probably associated with the limiting operating temperature of PVDF,[29,30] at which the polymer retains its properties due to the processes of restructuring occurring in it and the subsequent change in the state of aggregation. The onset of these processes is noted at temperatures of 138.5–145 °C, independent of the presence of other third-party components.[29] A further increase in temperature (up to 150–160 °C) leads to softening of PVDF as a result of melting. This, apparently, is the reason for the disappearance of the polar domains. It is clearly seen that up to this point $|d_{31}|$, $|g_{31}|$ and Q_M retain stable values. It is important to note that the piezoelectric activity of the sample was preserved after heating to 160 °C and then cooling to room temperature. In this case, the longitudinal piezomodule measured at room temperature, as well as at the limiting operating temperature, decreased by two times and amounted to $|d_{33}| = 15$ pC/N, despite the fact that at 160 °C the piezoproperties decreased by three times. The domain structure is probably partially restored upon cooling.

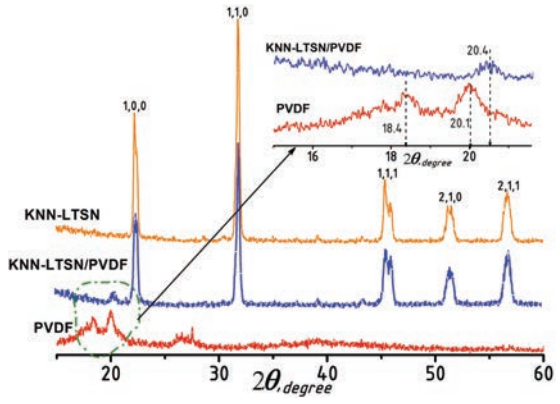

Fig. 4. Diffraction patterns of the investigated objects: pure KNN-LTSN and $(1-x)$[KNN-LTSN]–xPVDF with $x = 25$ vol.% and PVDF.

Figures 6 and 7 show the temperature–frequency dependences of the dielectric constant $\varepsilon'/\varepsilon_0(T)$ and the dielectric loss tangent $\mathrm{tg}\delta(T)$ of the $(1-x)$[KNN-LTSN]–xPVDF composite polymer ceramics at $x = 25$ vol.% and at $x = 50$ vol.% in the temperature range of $T = 26$–150 °C and the frequency range of $f = 20$–$2 \cdot 10^6$ Hz. The values are plotted on a logarithmic scale. At room temperature the ceramics were characterized by low values of the relative permittivity: $\varepsilon'/\varepsilon_0 = 230$–270 for $x = 25$ vol.% [Fig. 6(a)] and $\varepsilon'/\varepsilon_0 = 70$–110 for $x = 50$ vol.% [Fig. 6(b)] and low values of the dielectric loss tangent (up to 0.1) in both cases, which is a sufficiently large value for high through-conduction ceramics [$\gamma_s \sim 10^{-6}$ $(\Omega \cdot \mathrm{m})^{-1}$], giving a direct contribution $\gamma_s/(\varepsilon_0\omega)$ into the value of $\mathrm{tg}\delta$.[31] It is obvious that the dielectric constant increases with decreasing x, which is noted not only by us, but also in Ref. 30.

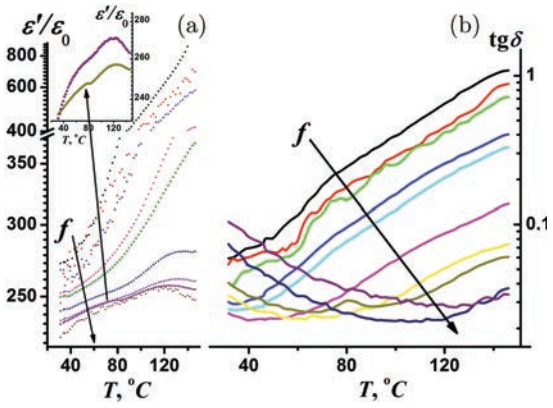

Fig. 6. Temperature–frequency dependences of (a) $\varepsilon'/\varepsilon_0(T)$ (a) and (b) tg$\delta(T)$ (b) on a logarithmic scale of (1–x)[KNN-LTSN]–xPVDF with x = 25 vol.%.

In both cases, the $\varepsilon'/\varepsilon_0(T)$ curves at high frequencies exhibit two relaxation maxima. Low-temperature diffuse maxima, clearly visible at frequencies f from 10^4 Hz to 10^6 Hz, are formed in the composite polymer ceramic (1–x)[KNN-LTSN]–xPVDF with x = 25 vol.% at T = 60–80 °C. With an increase in the polymer concentration to x = 50 vol.%, the temperature at which the first maxima appear decreases to T = 40–60 °C and the maxima themselves become more distinct. At a temperature of 120 °C, the second relaxation maxima T_m are clearly formed at x = 25 vol.% in the entire frequency range, while at PVDF concentration of x = 50 vol.% they are more diffuse.

The confirmation of the first relaxation process at low temperatures can be found in the dependences of tg$\delta(T)$ [Figs. 6(b) and 7(b)]. Here, it can be clearly seen the temperature evolution of tg$\delta(T)$ behavior at different frequencies. It should be noted that in (1–x)[KNN-LTSN]–xPVDF with x = 50 vol.% at low frequencies up to ~10^2 Hz at a temperature of 141 °C more relaxation maxima are formed, which possibly indicates a certain transition that precedes a sharp decrease in

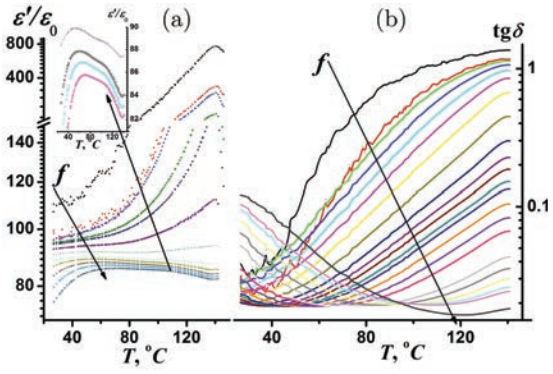

Fig. 7. Temperature–frequency dependences of (a) $\varepsilon'/\varepsilon_0(T)$ and (b) tg$\delta(T)$ on a logarithmic scale of (1–x)[KNN-LTSN]–xPVDF with x = 50 vol.%.

properties at the maximum working temperature of PVDF of T_{crit} = 150 °C (see Fig. 5).

The relaxation effects observed in the dielectric spectra of (1–x)[KNN-LTSN]–xPVDF are apparently associated with low density of the studied objects and weak interaction of the polymer with particles of the ferroelectric KNN-LTSN, as well as with the long-studied relaxation phenomena in PVDF films.[32–35] As it is known from the literature, although the polarization in PVDF is stable at room temperature, it relaxes if the temperature rises above ~80 °C (in the temperature range in which PVDF films can be polarized) without the application of an external field, which corresponds to that observed on Figs. 6 and 7 for the behavior of the dielectric spectra of the studied objects in the region of 80 °C. The relaxation rate and relaxation polarization depend on the annealing temperature and polarization conditions.[32,33] The dependence of the stability of the dipole moment on the polarization conditions can be associated with incomplete local compensation of the depolarizing field at the boundaries of crystals in matter, i.e., in the same way as in ceramics. Internal fields relax only at times longer than the dielectric relaxation time. In any case, macroscopic polarization appears to be metastable, even if the dipoles are ordered on a microscopic scale. There is no specific Curie temperature here. Dielectric studies of PVDF[32–35] make it possible to determine whether the Curie–Weiss law is satisfied or a pronounced dielectric anomaly in the temperature range where polarization relaxation is observed. In the range of 70–100 °C,[34] there is a wide maximum of dielectric losses, which is caused by molecular motion inside the crystalline regions of PVDF. The higher the degree of crystallinity of the film, the greater the dielectric loss and the higher the temperature of the loss peak,[35] which we observe in Fig. 7(b) at ~140 °C. Other loss maxima formed below room temperature are attributed to amorphous regions of the film and can explain the polarization effects that are observed in PVDF below room temperature.[35] As can be seen, in the region of ~25 °C at high frequencies, the tgδ maxima begin to form [Figs. 7(a) and 7(b)]. Obviously, as a result of some relaxation processes at low frequencies, they shift to temperatures below room temperature, which confirms the observed effects in PVDF films.[30]

Thus, we can conclude that in the dielectric spectra of the composite polymer ceramics (1–x)[KNN-LTSN]–xPVDF with x = 25 vol.% and 50 vol.%, three relaxation processes are observed in the temperature ranges of 40–80 °C, 80–120 °C and 120–150 °C, the description of which is very difficult within the framework of classical models. Therefore, to analyze such complex relaxation processes, we constructed frequency dependences of dielectric characteristics at different temperatures and applied to them the proven modified model (1), which we obtained earlier for complex conductivity based on the Havriliak–Negami formula.[17,18]

For example, Figs. 8 and 9 show the experimental frequency dependences of the real part of the dielectric constant $\varepsilon'/\varepsilon_0(f)$, the dielectric loss tangent tg$\delta(f)$, the real part of the

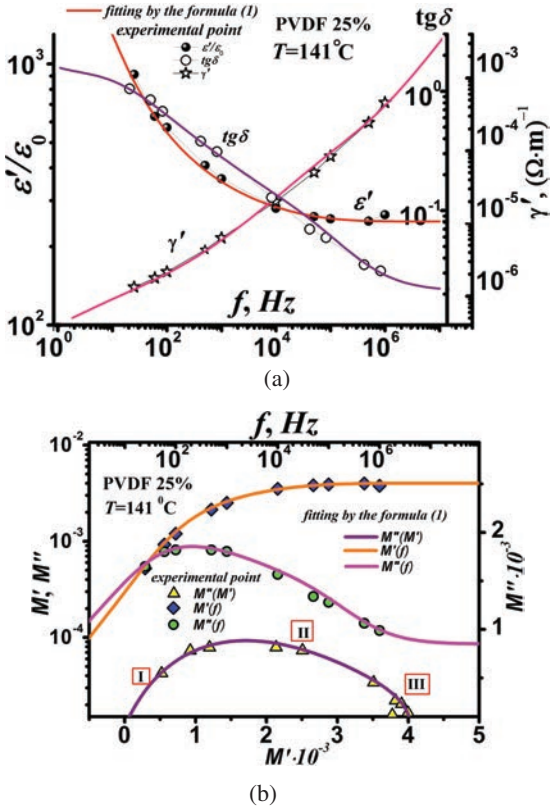

Fig. 8. Dependences of (a) $\varepsilon'/\varepsilon_0(f)$, tg$\delta(f)$ and $\gamma'(f)$ and (b) $M'(f)$, $M''(f)$ and $M''(M')$ of (1–x)[KNN-LTSN]–xPVDF (x = 25 vol.%) at T = 141 °C on a logarithmic scale.

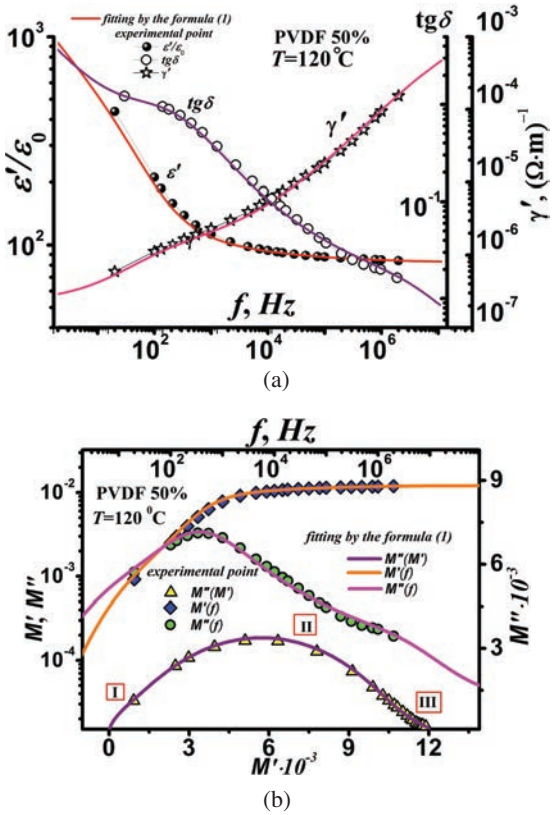

Fig. 9. Dependences of (a) $\varepsilon'/\varepsilon_0(f)$, tg$\delta(f)$, and $\gamma'(f)$ and (b) $M'(f)$, $M''(f)$ and $M''(M')$ of (1–x)[KNN-LTSN]–xPVDF (x = 50 vol.%) at T = 120 °C on a logarithmic scale.

complex electrical conductivity $\gamma'(f)$ as well as the Cole–Cole diagrams of (1–x)[KNN-LTSN]–xPVDF with x = 25 vol.% and 50 vol.% at temperatures of 141 °C and 120 °C, respectively. The form of the dependences $\varepsilon'/\varepsilon_0(f)$ and tg$\delta(f)$ indicates the occurrence of dielectric relaxation in the object, with a large contribution of the through electrical conductivity.

As can be seen, the approximation of the experimental points on all presented curves has a high degree of convergence, while three relaxation processes are observed, denoted by Roman numerals (I, II and III) on the $M''(M')$ dependences. Each of the processes was identified in the complex (and taking into account) of all the presented dependences in Figs. 8 and 9.

The first (I, 10^0–10^2 Hz) and third (III, 10^4–10^6 Hz) relaxation processes were obtained automatically with the combined use of formulas (1) and (2) and are predictive in nature, since the experimental points obtained in a wide frequency range are clearly smoothed process II. The second relaxation process (II) is clearly visible in the frequency range of 10^2–10^4 Hz. The obtained frequency ranges correlate well with the visible diffuse relaxing maxima in the corresponding frequency ranges on the $\varepsilon'/\varepsilon_0(T)$ dependences (Figs. 6 and 7).

To establish the dynamics of the transformation of frequency spectra at different temperatures, the composition (1–x)[KNN-LTSN]–xPVDF with x = 50 vol.% was chosen, as an object in which relaxation processes are clearly manifested. In total, the model (1) analyzed five temperature sections of the $\varepsilon'/\varepsilon_0(T)$ dependence (Fig. 7), the calculation results of which are presented in Table 1 and in Figs. 8 and 9.

Table 1. Main parameters, which were obtained from experimental data and calculated using formulas (1) and (2).

T (°C)	α	τ_1 (s)	τ_2 (s)	γ_s $(\Omega\cdot m)^{-1}$	$\gamma_{\infty 1}$ $(\Omega\cdot m)^{-1}$	γ_∞ $(\Omega\cdot m)^{-1}$	ε'_∞	ε''_∞	E_a (eV)
60	0.09	N/A	1.50E–08	4.00E–08	N/A	6.11E–03	75.78	0.0233	2.680
80	0.13	1.20E–03	1.80E–08	9.05E–08	3.80E–07	2.87E–03	80.62	0.0665	1.650
100	0.27	2.70E–03	4.40E–08	1.40E–07	6.95E–07	5.82E–04	83.74	0.1180	1.320
120	0.33	2.40E–03	3.40E–08	2.30E–07	1.71E–06	6.06E–04	83.05	0.2500	0.603
140	0.40	1.00E–03	2.40E–08	4.47E–07	5.72E–06	7.53E–04	81.66	0.3000	0.493

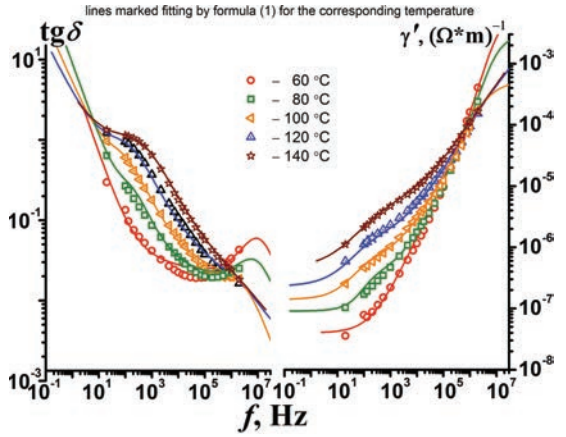

(a)

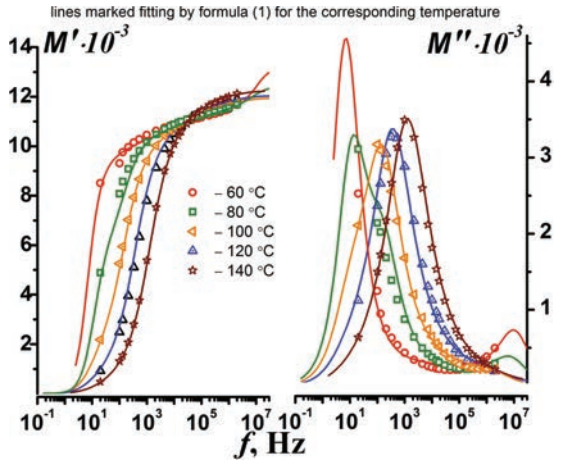

(b)

Fig. 10. Dependences of (a) tg$\delta(f)$ and $\gamma'(f)$ and (b) $M'(f)$ and $M''(f)$ on a logarithmic scale of (1–x)[KNN-LTSN]–xPVDF with x = 50 vol.% at different temperatures.

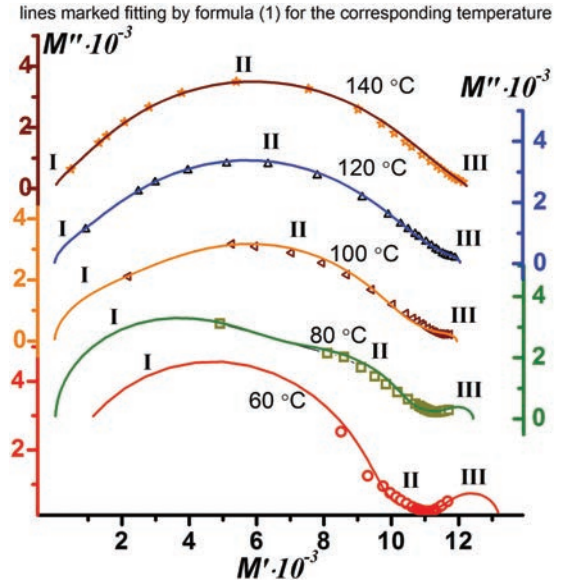

Fig. 11. Cole–Cole diagram of $M''(M')$ of (1–x)[KNN-LTSN]–xPVDF with x = 50 vol.% at different temperatures. Roman numerals indicate the numbers of relaxation processes.

It is seen that in all cases model (1) together with formula (2) also shows a high convergence of experimental points and approximation curves. Figures 10 and 11 show the dynamics of the transformation of three processes from 60 °C to 140 °C. This explains the presence of diffuse maxima of $\varepsilon'/\varepsilon_0(T)$ (Fig. 7). The first process (I) is clearly observed at low temperatures in the low-frequency range, which explains its absence in the $\varepsilon'/\varepsilon_0(T)$ dependence (Fig. 7) up to 140 °C. The second process (II) is weakly manifested at a temperature of 60 °C, it detects absorption by the processes I and III. However, it looks like a diagonal line between them. With an increase in temperature (after 80 °C), the process II opens up and by 140 °C is predominant absorbing the first and third processes.

Also, with an increase in temperature, processes I and III gradually decrease and at temperatures above 100 °C it is already noticeable in the region of 10^5 Hz in the frequency range under study and begins, as mentioned earlier in the description of how Fig. 7 looks in the low-frequency range, which explains the absence of the dependence of $\varepsilon'/\varepsilon_0(T)$ (Fig. 7) up to 140 °C. Observed in Figs. 10 and 11, the dynamics of changes in three relaxation processes proves the presence of the observed effects on the dependence $\varepsilon'/\varepsilon_0(T)$ (Figs. 6 and 7), and also shows the efficiency of the new model for describing complex dielectric spectra, any nonlinear dielectrics, including composite materials with any irregularities. All three relaxation processes correlate well with the data obtained in other composites made in the form of thin films.[30]

In conclusion, we note that the increasing values of M' with increasing frequency indicate the S-shaped dispersion of M', which is typical for materials with ionic conductivity.[36,37] This fact is also confirmed by the calculated values of the activation energy given in Table 1, which increase with increasing temperature due to an increase in the through electrical conductivity. In polymer composites, the presence of various inclusions leads to the appearance of interfacial polarization by the so-called Maxwell–Wagner–Sillers effect.[38] This phenomenon occurs in heterogeneous media due to the accumulation of charges at the interfaces.

4. Conclusions

Composite polymer ceramics (1–x)[KNN-LTSN]–xPVDF at x = 25 vol.% (ρ = 3.17 g/cm^3, $|d_{33}|$ = 30 pC/N) and x = 50 vol.% (ρ = 3.24 g/cm^3, $|d_{33}|$ = 9 pC/N) are studied. It is shown its they have fairly stable piezoelectric properties in the temperature range of 26–80 °C. This indicates the possibility of modernizing technological processes by reducing

the temperature and time of obtaining the final stage of the material (~1200 °C) by 3–4 times due to the use of PVDF as a binder. It is noted that the magnitude of the piezomodule of lead-free composite materials with PVDF has an exponential dependence on the polymer concentration. However, this requires additional research to establish sintering modes.

The analysis of the piezomodules made it possible to conclude that due to a decrease in the PVDF content, as well as an increase in the temperature and pressing pressure, their optimal values can be achieved. In addition, a decrease in the size of granules of the piezoactive phase due to, e.g., the use of the method of mechanical activation can also lead to a denser electromechanical interaction of KNN-LTSN fragments, which, along with an increase in the experimental density, will contribute to an increase in piezoelectric coefficients.

It was established by X-ray diffraction methods that the α-phase (18.4°) of PVDF, which is the reason for the low dielectric activity of it due to the nonpolar chain crystalline conformation, disappears during preparation of the (1–x)[KNN-LTSN]–xPVDF composite. It was also found that the β-phase reflex shifts from ~20.1° to ~20.4°. This indicates a partial reaction of the polymer with KNN-LTSN particles, which leads to a slight decrease in its structural parameters.

Investigations of dielectric spectra in wide ranges of temperatures and frequencies were carried out using an experimental model for describing complex electrical conductivity based on the Havriliak–Negami formula. It was noted that in spite of their extremely complex relaxation character, the description of which is very difficult within the framework of classical models, with the help of this formula it was possible to achieve almost complete convergence with experiment. It is shown that the temperature–frequency spectra include three relaxation processes in the temperature ranges of 40–80 °C, 80–120 °C and 120–150 °C, which were confirmed by the dynamics of changes in the dependences of $\gamma'(f)$, tg$\delta(f)$, $M'(f)$, $M''(f)$ and $M''(M')$. All three relaxation processes correlate well with the work of researchers studying other composites based on PVDF, including those made in the form of thin films.

Thus, the studies carried out show that the modernized Havriliak–Negami model can be used to describe the complex dielectric spectra of any nonlinear dielectrics, including composite materials.

Acknowledgments

This work was financially supported by the Ministry of Science and Higher Education of the Russian Federation: State Task in the Field of Scientific Activity, Scientific Project No. 0852-2020-0032 (BAZ0110/20-3-07IF) with the use of equipment of the Center for Collective Use "Integrated Centre of Scientific-Technological Equipment SSC RAS (Research, Development, Approval)", Southern Scientific Centre of RAS (No. 501994). The dielectric measurements were performed using the equipment of the Shared Research Facility Centre of SFedU, Research Institute of Physics.

References

[1]A. A. Nesterov, V. Yu. Topolov, M. I. Tolstunov and A. N. Isaeva, Longitudinal piezoelectric effect and hydrostatic response in novel laminar composites based on ferroelectric ceramics, *Ceram. Int.* **45**(17), 22241 (2019), doi:10.1016/j.ceramint.2019.07.248.

[2]V. Yu. Topolov and A. N. Isaeva, Comparison of effective parameters of lead-free 1–3-type composites based on ferroelectric single crystals, *Ferroelectrics* **567**(1), 182 (2020), doi:10.1080/0015019 3.2020.1791602.

[3]E. K. Akdogan, M. Allahverdi and A. Safari, Piezoelectric composites for sensor and actuator applications, *IEEE Trans. Ultrason. Ferroelectr. Freq. Control* **52**, 746 (2005).

[4]A. N. Rybyanets and A. A. Naumenko, Nanoparticles transport in ceramic matrixes: A novel approach for ceramic matrix composites fabrication, *J. Mod. Phys.* **4**, 1041 (2013), doi:10.1007/978-0-387-76540-2_15.

[5]J. B. Lando, H. G. Olf and A. Peterlin, Nuclear magnetic resonance and X-ray determination of the structure of poly(vinylidene fluoride), *J. Polym. Sci. A* **4**(4), 941 (1966).

[6]V. Kumar *et al*., On nanographene-reinforced polyvinylidene fluoride composite matrix for 4D applications, *J. Mater. Eng. Perform.* (2021), doi:10.1007/s11665-021-05459-z.

[7]M. U. Abba *et al*., Novel PVDF-PVP hollow fiber membrane augmented with TiO_2 nanoparticles: Preparation, characterization and application for copper removal from leachate, *Nanomaterials* **11**, 399 (2021), doi:10.3390/nano11020399.

[8]K. Gurpreet and D. S. Rana, Designing of pressure sensor with polyvinylidene fluoride composite films embedded with nickel oxide for energy harvesting, *Mater. Today, Proc.* **45**, 4458 (2021), doi:10.1016/j.matpr.2020.12.839.

[9]K. Gurpert and D. S. Rana, Synthesis and comprehensive investigation on structural, morphological and electrical properties of PVDF-$BaTiO_3$ nanocomposite films, *Optoelectron. Adv. Mater. — Rapid Commun.* **14**(11–12), 542 (2020).

[10]S. Mohanty, V. Panwar and P. Khanduri, Development of flexible piezoresistive dielectric membrane by PVDF/Fe_3O_4, *Mater. Today, Proc.* **44**, 1707 (2020), doi:10.1016/j.matpr.2020.11.876.

[11]V. Rathi *et al*., PVDF/CNF/IL composite film for shielding of microwave radiation, *Mater. Today, Proc.* (2021), doi:10.1016/j.matpr.2020.12.483.

[12]Y. Niu, K. Yu, Y. Bai and H. Wang Enhanced dielectric performance of $BaTiO_3$/PVDF composites prepared by modified process for energy storage applications, *IEEE Trans. Ultrason. Ferroelectr. Freq. Control* **62**, 108 (2015), doi:10.1109/TUFFC.2014.006666.

[13]S. Bairagi and S. Wazed Ali, Flexible lead-free PVDF/SM-KNN electrospun nanocomposite based piezoelectric materials: Significant enhancement of energy harvesting efficiency of the nanogenerator, *Energy* **198**(1), 117385 (2020), doi:10.1016/j.energy.2020.117385.

[14]The European Parliament and The Council of the European Union, Directive 2002/95/EC of the European Parliament and of the Council of 27 January 2003 on the re-striction of the use of certain hazardous substances in electronic equipment, *Off. J. Eur. Union* **37**, 19 (2003).

[15]I. A. Verbenko, O. N. Razumovskaya, L. A. Shilkina, L. A. Reznichenko and K. P. Andryushin, Production and dielectric properties of lead-free ceramics with the formula $[(Na_{0.5}K_{0.5})_{1-x}Li_x]$-$(Nb_{1-y-z}Ta_ySb_z)O_3$, *Inorg. Mater.* **45**(6), 702 (2009).

[16]L. A. Reznichenko, I. A. Verbenko, A. V. Pavlenko, S. N. Dudkina and N. A. Boldyrev, A lead-free piezoelectric ceramic material, Russian Patent No. 2571465 (2019).

[17]Y. I. Yurasov and A. V. Nazarenko, Parameter of dielectric loss distribution in the new model for complex conductivity based on Havriliak–Negami formula, *J. Adv. Dielectr.* **10**(1–2), 2060006 (2020).
[18]Y. I. Yurasov and A. V. Nazarenko, A new approach to dielectric spectra description based on the Havriliak-Negami model, *Nauka Yuga Rossii* **14**(4), 35 (2018).
[19]Y. I. Yurasov, A. V. Pavlenko and A. V. Nazarenko, Knock sensor, Russian Patent No. 158291 (2015).
[20]Y. I. Yurasov, A. V. Pavlenko, I. A. Verbenko, H. A. Sadykov and L. A. Reznichenko, Knock sensors based on lead-free piezoceramics, *Compos. Mater. Construct.* **4**(140), 81 (2015).
[21]Y. I. Yurasov, A. V. Nazarenko, A. V. Pavlenko and I. A. Verbenko, Prediction of the properties of lead-free piezoceramics and modification of the construction of vibration sensors based on lead-containing compositions, *Nauka Yuga Rossii* **13**(4), 23 (2017).
[22]I. N. Andryushina *et al*., The PZT system ($PbTi_xZr_{1-x}O_3$, $0 \le x \le 1.0$): Dielectric response of solid solutions in broad temperature ($10 \le T \le 1000$ K) and frequency ($10^{-2} \le f \le 10^7$ Hz) ranges (part 4), *Ceram. Int.* **39**(4), 3979 (2013), doi:10.1016/j.ceramint.2012.10.246.
[23]The Institute of Electrical and Electronics Engineers, ANSI/IEEE Standard 176–1987: IEEE standard on piezoelectricity, New York (1988).
[24]ALGLIB Project, ALGLIB numerical analysis library (2021), http://www.alglib.net/.
[25]Y. I. Yurasov, A. V. Pavlenko and A. V. Nazarenko, Program for predicting the frequency dependences of the dielectric spectra and electrical conductivity of ferroelectric materials depending on the temperature and activation energy, taking into account the Havriliak-Negami model, Program for PC No. 2019610938 (2019).
[26]M. Alexandre, C. Bessaguet, C. David, E. Dantras and C. Lacabanne, Piezoelectric properties of polymer/lead-free ceramic composites, *Phase Trans.* **89**(7–8), 708 (2016), doi:10.1080/01411594.2016.1206898/.
[27]A. N. Arshad, M. H. M. Wahid, M. Rusop, W. H. A. Majid, R. H. Y. Subban and M. D. Rozana, Dielectric and structural properties of poly(vinylidene fluoride) (PVDF) and poly(vinylidene fluoride-trifluoroethylene) (PVDF-TrFE) filled with magnesium oxide nanofillers, *J. Nanomater.* **2019**, 5961563 (2019), doi:10.1155/2019/5961563.
[28]A. Lund, C. Gustafsson, H. Bertilsson and R. W. Rychwalski, Enhancement of β-phase crystals formation with the use of nanofillers in PVDF films and fibres, *Compos. Sci. Technol.* **71**(2), 222 (2011).
[29]Z. Liu, P. Maréchal and R. Jérôme, Melting and crystallization of poly(vinylidene fluoride) blended with polyamide 6, *Polymer* **38**(20), 5149 (1997), doi:10.1016/S0032-3861(97)00047-5.
[30]L. Zhang, Z. Liu, X. Lu, G. Yang, X. Zhang and Z.-Y. Cheng, Nanoclip based composites with a low percolation threshold and high dielectric constant, *Nano Energy* **26**, 550 (2016), doi:10.1016/j.nanoen.2016.06.022/.
[31]A. S. Bogatin and A. V. Turik, *Processes of Relaxation Polarization in Dielectrics with Large Through Conductivity* (Feniks Press, Rostov-on-Don, Russia, 2013).
[32]A. M. Glass, J. H. McFee and J. G. Bergman, Pyroelectric properties of polyvinylidene fluoride and its use for infrared detection, *J. Appl. Phys.* **42**, 5219 (1971).
[33]G. Pjister, M. A. Abkowitz and R. G. Crystal, Pyroelectricity in polyvinylidene fluoride, *J. Appl. Phys.* **44**, 2064 (1973).
[34]H. Sasabe, S. Saito, M. Asahina and H. Kakutani, Dielectric relaxations in poly(vinylidene fluoride), *J. Polym. Sci. A* **7**(8), 1405 (1969).
[35]G. Pfister and A. Abkowitz, Dipole reorientation in polyvinylidene fluoride, *J. Appl. Phys.* **45**, 1001 (1971).
[36]S. El-Sayed, T. A. Abdel-Baset and A. Hassen, Dielectric properties of PVDF thin films doped with 3 wt.% of RCl_3 (R = Gd or Er), *AIP Adv.* **4**, 037114 (2014), doi:10.1063/1.4869093.
[37]M. F. Mostafa and A. Hassen, Phase transition and electric properties of long chain Cd(II) layered perovskites, *Phase Trans.* **79**, 305 (2006), doi:10.1080/01411590600670237.
[38]A. Hassen, T. Hanafy, S. El-Sayed and A. Himanshu, Dielectric relaxation and alternating current conductivity of polyvinylidene fluoride doped with lanthanum chloride, *J. Appl. Phys.* **110**, 114119 (2011), doi:10.1063/1.3669396.